Three-Dimensional Molecular Alignment Inside Helium Nanodroplets

Adam S. Chatterley, Benjamin Shepperson, and Henrik Stapelfeldt
Department of Chemistry, Aarhus University, Langelandsgade 140, DK-8000 Aarhus C, Denmark
(Received 6 April 2017; published 14 August 2017)

We demonstrate 3D spatial alignment of 3,5-dichloroiodobenzene molecules embedded in helium nanodroplets using nonresonant elliptically polarized 160 ps laser pulses at a 1 kHz repetition rate. Through Coulomb explosion imaging and ion-ion covariance mapping, the 3D alignment is characterized and found to be stronger than that of isolated molecules. The 3D alignment follows the intensity profile of the alignment laser pulse almost adiabatically, except for a delayed response in the helium droplets, which could be exploited for field-free 3D alignment. Our results pave the way for next-generation molecular dynamics and diffraction experiments, performed within a cold helium solvent.

DOI: 10.1103/PhysRevLett.119.073202

Controlling the spatial alignment of molecules in three dimensions is of central importance to a range of areas in molecular science, including ultrafast reaction dynamics [1], tomographic imaging [2], strong-field ionization [3], and x-ray diffraction [4], primarily because it maximizes the information content of experimental observables through molecular frame measurements. Three-dimensional alignment of isolated gas phase molecules has been demonstrated using the interaction of moderately intense laser fields with molecules in several different schemes [5,6]. These encompass adiabatic alignment using elliptically polarized nanosecond pulses [7–9], field-free nonadiabatic alignment using sequences of femtosecond laser pulses [10–13], hybrid approaches where both adiabatic and nonadiabatic alignment are employed simultaneously [14,15], an optical centrifuge [16], and switched wave packet methodology, [17] where a pulse with a nanosecond rise time, but subpicosecond fall time, was employed to obtain field-free alignment [18].

All previous 3D alignment experiments and theory were performed on isolated molecules. Recently, it was demonstrated that laser-induced 1D alignment, both in the nonadiabatic and adiabatic regimes, can be achieved for molecules embedded in superfluid helium droplets [19–23]. This extension of molecular alignment from the gas phase to inside He droplets represents several advantages, and motivates the current work. First, the 0.4 K temperature of molecules in He droplets [24] should be more favorable for creating strong alignment. This was demonstrated recently in the near-adiabatic regime where very high degrees of 1D alignment were reported for different molecules in He droplets—significantly surpassing the alignment obtained for molecules in a cold molecular beam under identical laser conditions [23]. Second, He droplets give access to studies on clusters, complexes, and large molecules that are often very difficult to form otherwise—in particular, at a low temperature [25]. Third, molecules in He droplets enable molecular dynamics experiments in the presence of a dissipative environment [19].

These points strongly motivate exploring if, and to what extent, 3D alignment can be realized in He droplets. In particular, an improvement of the degree of alignment compared to that achievable in the gas phase would be most important for experiments which require samples of very tightly aligned molecules to succeed. This is the case for diffractive imaging with ultrashort electron or x-ray pulses aimed at extraction of accurate molecular structure information, and the use of He droplet environments has already been proposed for such studies [26–28].

Here, we demonstrate that 3D alignment of molecules embedded inside helium nanodroplets is possible, using 3,5-dichloroiodobenzene (DCIB) as an example. The alignment is achieved adiabatically employing 160 ps long, elliptically polarized pulses. The degree of alignment achieved is high, and after correcting for nonaxial recoil effects, we find it exceeds that of isolated molecules in a cold molecular beam.

The details of the experimental setup are given elsewhere [23], so the description here is brief. A beam of helium droplets is produced from a continuous expansion into vacuum of 25 bar He gas through a 5 μm nozzle precooled to 13 K. At this temperature each droplet contains on average $\sim 8 \times 10^3$ helium atoms [29]. To dope DCIB molecules into the droplets, they are sent through a pickup cell, whose pressure of DCIB is adjusted to maximize single molecule doping. Hereafter, the doped He droplet beam enters the target region inside a velocity map imaging spectrometer, where it is crossed at 90° by two pulsed laser beams. One beam, stemming from the uncompressed output of a Ti:sapphire regenerative amplifier, is used for molecular alignment [30,31]. These alignment pulses centered at $\lambda = 800\,\text{nm}$ are highly chirped (GDD $= +1.7$ ps^2), 160 ps (FWHM), focused to a Gaussian spot size, $\omega_0 = 27$ μm and have a peak intensity $I_{\text{align}} = 1.1 \times 10^{12}$ W/cm^2. Their polarization is controlled by a quarter wave plate preceded by a half wave plate. The other beam consists of 35 fs probe pulses ($\omega_0 = 18$ μm, $I_{\text{probe}} = 5.3 \times 10^{14}$ W/cm^2,

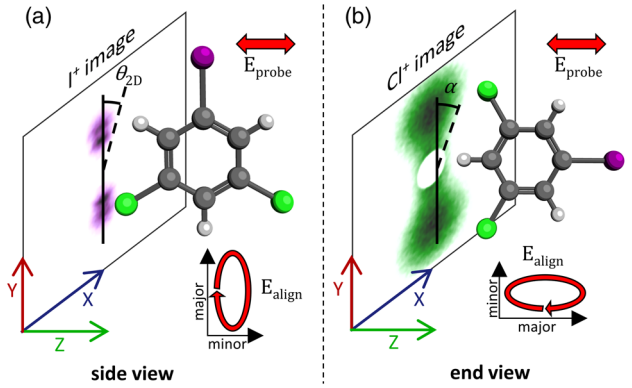

FIG. 1. Illustration demonstrating the projection of the molecular alignment onto observed ion images. (a) I^+ image (purple) recorded in the side view obtained by directing the major polarization axis of the alignment pulse parallel to the detector. (b) Cl^+ image (green) recorded in the end view obtained by directing the major polarization axis of the alignment pulse perpendicular to the detector.

$\lambda_{\text{center}} = 800$ nm), used to measure the degree of alignment by Coulomb explosion and detection of the emission direction of fragment ions. The ions of interest here, I^+ and Cl^+, are velocity map imaged onto a position sensitive detector [32], which is gated in time to detect only ions of a single mass. A second molecular beam, containing jet-cooled isolated DCIB molecules, can be sent into the target region. This allows recording alignment of gas phase molecules under identical laser pulse conditions.

The principle of the 3D alignment scheme applied here is to simultaneously confine the most polarizable axis of the DCIB molecule along the major polarization axis of the alignment pulse, and the second most polarizable axis along the minor polarization axis of the alignment pulse, through the polarizability interaction between the elliptically polarized alignment pulse and the molecule [7]. As the molecule is rigid, the least polarizable axis is automatically confined, and the molecule is 3D aligned. For DCIB, the most polarizable axis is parallel to the C – I axis and the second most polarizable axis is parallel to the Cl-Cl axis—see the schematic of the molecular structure in Fig. 1.

Following experience from previous experiments on isolated molecules, we record the I^+ ions from the Coulomb explosion in the side view and the Cl^+ ions in the end view, because this gives the highest information about the molecular alignment [9,14]. Here, side view and end view refer to the C – I axis being parallel or perpendicular to the detector plane. In practice, this is obtained by directing the major polarization axis of the alignment pulse parallel (side view) or perpendicular (end view) to the detector plane, as illustrated in Fig. 1. In both views the polarization axis of the linearly polarized probe pulse is kept perpendicular to the detector plane. All I^+ (Cl^+) images are presented in a purple (green) color in the side (end) view.

Images of I^+ and Cl^+ ions from Coulomb explosion of DCIB molecules embedded in He droplets are displayed in the upper panel of Fig. 2. For all the data shown, the probe pulse is synchronized to the peak of the alignment pulse. With a linearly polarized alignment pulse [Fig. 2(a)], the I^+ ions recorded fall primarily in two regions localized along the polarization direction. In analogy with previous studies we interpret this as 1D alignment, where the C – I axis is confined along the polarization vector of the alignment pulse. The degree of alignment is quantified by $\langle\cos^2\theta_{2D}\rangle$, where θ_{2D} is the angle between the projection of an I^+ velocity vector on the detector plane and the polarization vector of the alignment pulse; see Fig. 1(a). The value of $\langle\cos^2\theta_{2D}\rangle$ is 1 for perfectly aligned molecules and, with the probe pulse polarized perpendicular to the detector plane, 0.5 for randomly aligned molecules. To ensure that we only include I^+ ions from the Coulomb explosion process, $\langle\cos^2\theta_{2D}\rangle$ is determined from the ions with a radii greater than the blue annotated circle, and the value obtained is $\langle\cos^2\theta_{2D}\rangle = 0.85$. The corresponding Cl^+ image [Fig. 2(e)] is circularly symmetric, which we interpret as the Cl-Cl axis, and thus the plane, of the molecules uniformly distributed around the Z axis. This is fully compatible with the C – I axis being aligned perpendicular to the detector plane.

Next, we investigate the effect of an elliptically polarized alignment pulse. For an ellipticity intensity ratio of 3.7:1 the Cl^+ image [Fig. 2(f)] is no longer circular symmetric, but rather localized along the minor polarization axis [the Y axis in Fig. 1(b)]. The localization is quantified by $\langle\cos^2\alpha\rangle$, where α is the angle between the projection of a Cl^+ velocity vector on the detector plane and the minor polarization vector of the alignment pulse [Fig. 1(b)], determined from the Cl^+ ions outside the blue annotated circle. The value of $\langle\cos^2\alpha\rangle$ is 0.67, compared to 0.49 with the linearly polarized alignment pulse. Turning to the I^+ image, Fig. 2(b), it is almost identical to the image obtained with linear polarization; i.e., the C – I axis is still aligned. The joint observations from the Cl^+ and the I^+ images show that the DCIB moleules inside He droplets are 3D aligned with the C – I axis confined along the major polarization axis and the Cl-Cl axis confined along the minor axis.

Figures 2(c) and 2(g) show the I^+ and Cl^+ images recorded for another ellipticity, with an intensity-ratio of 1.7:1. The qualitative structures of the images are similar to the images recorded with the 3.7:1 ratio, but the confinement of the Cl-Cl axis is more pronounced, as shown by the increased value of $\langle\cos^2\alpha\rangle$ to 0.75. We interpret this as the result of the higher intensity along the minor polarization, similar to previous observations for gas phase molecules [9]. Finally, the I^+ and Cl^+ images were recorded for a circularly polarized alignment field. Unlike the cases for the elliptically polarized fields, the radial distributions of both ion species no longer form two separated regions, instead appearing as a blurred streak, although angular confinement persists. We interpret these observations as the

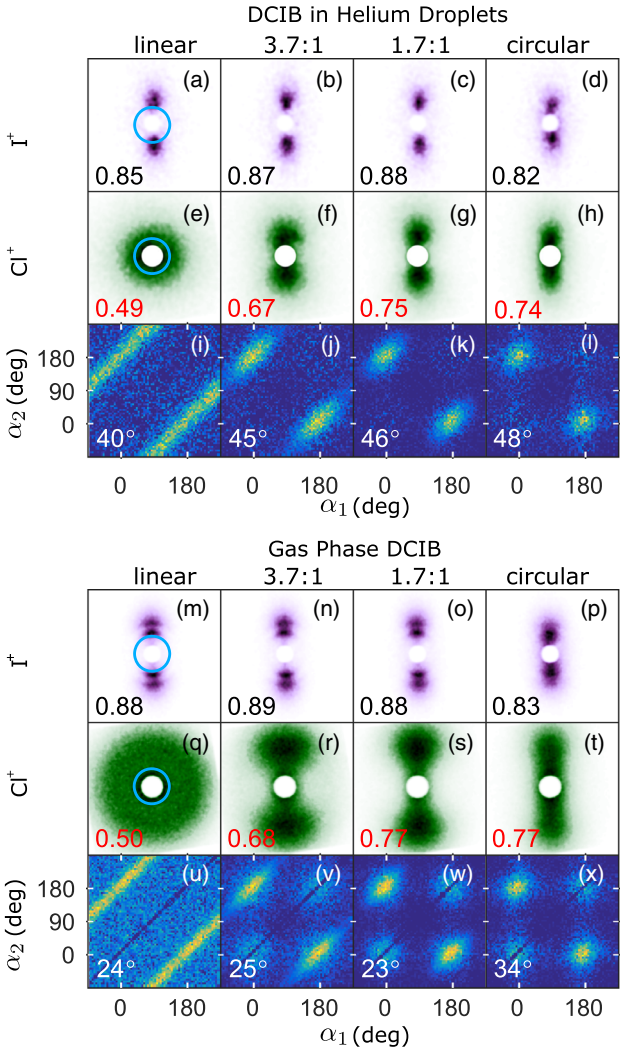

FIG. 2. I^+ images, (a)–(d), and Cl^+ images, (e)–(h), from DCIB molecules in He droplets with the polarization state of the alignment pulse, ranging from linear to circular, indicated above. On each panel the value of $\langle\cos^2\theta_{2D}\rangle$ ($\langle\cos^2\alpha\rangle$) is shown for the I^+ images (Cl^+ images), calculated using all events with a radius larger than the blue circles in (a) and (e). (i)–(l) Angular covariance maps of the Cl^+ images in panel (e)–(h). α_1 and α_2 both refer to the angle defined in Fig. 1(b). The number in each panel is the width w of the covariance structures (see text for details). Panels (m)–(x) are the same as panels (a)–(l) but for isolated DCIB molecules.

molecular plane being confined to the polarization plane of the alignment pulse, with the C – I axis of the molecules uniformly distributed in this plane.

To benchmark the 3D alignment of DCIB molecules in helium droplets, we also performed experiments on isolated DCIB molecules under identical conditions of the laser pulses. The images of both I^+ and Cl^+ are presented in Figs. 2(m)–2(t). Compared to the images recorded for molecules in He droplets, identical trends are observed, in particular, pronounced localization of the I^+ and the Cl^+ ions along the major and minor polarization axis, respectively, for an elliptically polarized alignment pulse. The values of $\langle\cos^2\theta_{2D}\rangle$ and $\langle\cos^2\alpha\rangle$ are very close to those observed for the droplet case. The I^+ images show two radially distinct channels. They result from Coulomb explosion into an I^+ ion with a $C_6H_4Cl_2^+$ or $C_6H_4Cl_2^{2+}$ partner [14,33]. These channels are not resolved for the He droplet case, due to the scattering of the I^+ ions as they exit the droplet.

In all alignment experiments on polyatomic molecules probed using Coulomb explosion imaging, the observed alignment metrics, like $\langle\cos^2\theta_{2D}\rangle$ and $\langle\cos^2\alpha\rangle$, reflect both the molecular alignment distribution, and nonaxial recoil (NAR) [34–36]. Nonaxial recoil refers to the deviation of the fragment ion's recoil vector from the direction of the bond it formed with the molecule—typically caused by vibrations or asymmetric Coulomb explosion processes, or for molecules within droplets, scattering off of helium atoms [37]. Separating the two contributions is essential for evaluating the true degree of alignment. For 1D alignment, NAR has previously been described both for isolated and helium solvated molecules, and its effect could be deconvoluted to derive the true degree of molecular alignment [37]. Here, we extend this analysis to 3D alignment and correct the observed values of $\langle\cos^2\theta_{2D}\rangle$ and $\langle\cos^2\alpha\rangle$.

To estimate the NAR of the Cl^+ ions, we apply angular covariance analysis of the Cl^+ ions [37–39]. The results are displayed as angular covariance maps in Figs. 2(i)–2(l) and 2(u)–2(x). For the linearly polarized alignment pulse, the covariance maps [panels (i) and (u)] contain two prominent diagonal streaks centered at $\alpha_2 = \alpha_1 + 180°$ and $\alpha_2 = \alpha_1 - 180°$ with a uniform distribution over the entire angular range. This shows that the two Cl^+ ions are emitted with a relative angle of 180° with no preference for absolute emission angle—the latter observation being a consequence of the circularly symmetric Cl^+ images in Figs. 2(e) and 2(q). As the alignment pulse polarization is changed to elliptical, and eventually circular, the streaks change into islands localized around 0° and 180°, reflecting the confinement of the Cl^+ ions along the minor polarization axis in the images shown in Figs. 2(f)–2(h) and 2(r)–2(t).

The width w of the covariance islands stays, however, approximately constant shown by the value given on each covariance map. As discussed in the Supplemental Material [40] the width extracted for the 1D aligned case, 40° (24°) for the He droplets (gas phase), represents the most accurate measure of the NAR. The larger width for the droplet case results from scattering of the departing ions on the He atoms. Using these values we deconvoluted the NAR from the angular distributions of the Cl^+ ions using the method described in Ref. [37] and obtained the following values (with 95% confidence bounds): $\langle\cos^2\alpha\rangle_{gas} = 0.761 \pm 0.002 (0.832 \pm 0.002)$ and $\langle\cos^2\alpha\rangle_{He} = 0.778 \pm 0.005 (0.860 \pm 0.006)$ for the 3.7:1 (1.7:1) ellipticity ratio. This shows that the molecular plane is better aligned for the molecules inside the He droplets, which we ascribe to the lower rotational temperature (0.4 K) for the

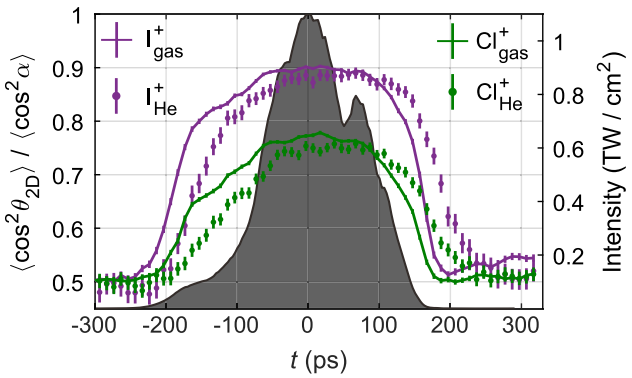

FIG. 3. The time dependence of $\langle\cos^2\alpha\rangle$ and $\langle\cos^2\theta_{2D}\rangle$ induced by a 1.7:1 elliptically polarized alignment pulse for both isolated molecules and molecules in He droplets. The intensity profile of the alignment pulse is shown by the shaded gray area and refers to the right vertical axis. The error bars are 95% confidence intervals.

molecules in the droplets compared to molecules in the molecular beam (~1 K) [23].

For the I^+ fragments it is not possible to use the covariance method to measure the NAR since there is only a single iodine atom in the DCIB molecule. As a substitute, we use the NAR of 1D aligned 1,4-diiodobenzene, which has previously been measured as 34° and 21° for the helium and gas environments, respectively [37]. We expect that these values may underestimate the NAR in DCIB, since 1,4-diiodobenzene is a more symmetric molecule; however, they should provide an acceptable first order correction. As these values are estimates, we do not give precise confidence intervals. Applying the deconvolution procedure, we retrieve corrected $\langle\cos^2\theta_{2D}\rangle$ values of $\langle\cos^2\theta_{2D}\rangle_{gas} = 0.94(0.94)$ and $\langle\cos^2\theta_{2D}\rangle_{He} = 0.96(0.96)$, in the 3.7:1 (1.7:1) ellipticity case; i.e., the C − I axis is also better aligned for the molecules inside the droplets. The overall conclusion from the covariance analysis of the Cl^+ and I^+ images is that molecules inside He droplets are better 3D aligned than the isolated molecules.

Finally, we turn to the time dependence of the 3D alignment obtained by recording I^+ and Cl^+ images at a range of different delays t between the probe pulse and the center of the alignment pulse. Figure 3 shows $\langle\cos^2\theta_{2D}\rangle$ and $\langle\cos^2\alpha\rangle$ as a function of time in both gas and helium environments for the 1.7:1 ellipticity. No correction for NAR was performed. The gray shaded area represents the temporal shape of the alignment pulse, determined by cross-correlation with the probe pulse in a nonlinear crystal. In the gas phase, both $\langle\cos^2\theta_{2D}\rangle$ and $\langle\cos^2\alpha\rangle$ follow the envelope of the pulse, reaching the highest values at the peak of the pulse—a behavior characteristic of adiabatic alignment [41–44]. For the DCIB molecules in He droplets, $\langle\cos^2\theta_{2D}\rangle$ and $\langle\cos^2\alpha\rangle$ also follow the pulse shape, but compared to the gas phase results the curves are shifted to later times. This finding suggests that the helium environment impedes the rotational motion of the molecule [19]. Similar observations were made for 1D alignment of I_2 molecules in He droplets with the same pulse shape [23].

The impeded rotational motion could potentially be exploited as a route to field-free 3D alignment, and in fact our data already show the potential for this. For instance, at $t = 170$ ps, where the intensity has dropped to <1% of the peak value, $\langle\cos^2\theta_{2D}\rangle = 0.76$, and $\langle\cos^2\alpha\rangle = 0.63$ for the molecules in the droplets; i.e., there is still appreciable alignment. The switch-off time of the pulse is currently more than 100 ps; however, if it was reduced to ~1 ps, then the adiabatically built-up 3D alignment should retain its high level for several picoseconds, under conditions where the alignment field is negligible for most applications. Such pulses have previously been produced using the plasma shutter technique to truncate a nanosecond pulse with a synchronized femtosecond laser pulse [17,18]; however, the picosecond alignment pulses employed here could potentially be shaped by simpler means. For the very chirped alignment pulse used here, the spectral and temporal shapes correspond approximately linearly. A sharp cutoff in temporal pulse shape can thus be produced by inserting a very sharp-edged low (high) pass spectral filter into the beam path for a positively (negatively) chirped alignment pulse [45]. We are currently performing experiments to test whether field-free 3D alignment can be produced in this manner.

In conclusion, we have shown that laser-induced 3D alignment is possible for molecules inside He nanodroplets. Our studies employed 3,5-dichloroiodobenzene molecules as an example and essentially identical results were obtained on 3,5-difluoroiodobenzene molecules. The helium droplet environment offers several interesting advantages for applications of 3D aligned molecules compared to studies in molecular beams. First, in the adiabatic alignment regime explored here the degree of alignment is determined by the temperature for a molecule at a given laser intensity. Therefore, molecules in He droplets will, in general, align better than gas phase molecules under identical laser conditions, as demonstrated here, because the temperature of the latter only rarely reach the 0.4 K of He droplets. Second, the strong alignment may be converted to field-free alignment by switching off the alignment field through simple spectral modification. The impeding effect of the He environment on the rotational motion should retain the field-free alignment for times long enough to allow molecular frame, time-resolved imaging of molecules during chemical changes. Third, helium droplets extend the range of molecules amenable to alignment, in particular to large (bio)molecules and to complexes built by doping with different molecules [46,47]. The latter may provide unique opportunities for performing chemistry in a controlled environment [29,48] and the ability to 3D align molecular complexes could be highly useful for imaging their structure.

We acknowledge support from the European Research Council-AdG (Project No. 320459, DropletControl) and the Villum Foundation.

[1] L. Christensen, J. H. Nielsen, C. B. Brandt, C. B. Madsen, L. B. Madsen, C. S. Slater, A. Lauer, M. Brouard, M. P. Johansson, B. Shepperson, and H. Stapelfeldt, Phys. Rev. Lett. **113**, 073005 (2014).

[2] J. Maurer, D. Dimitrovski, L. Christensen, L. B. Madsen, and H. Stapelfeldt, Phys. Rev. Lett. **109**, 123001 (2012).

[3] L. Holmegaard, J. L. Hansen, L. Kalhoj, S. Louise Kragh, H. Stapelfeldt, F. Filsinger, J. Küpper, G. Meijer, D. Dimitrovski, M. Abu-samha, C. P. J. Martiny, and L. Bojer Madsen, Nat. Phys. **6**, 428 (2010).

[4] D. Rolles *et al.*, J. Phys. B **47**, 124035 (2014).

[5] M. Lemeshko, R. V. Krems, J. M. Doyle, and S. Kais, Mol. Phys. **111**, 1648 (2013).

[6] H. Stapelfeldt and T. Seideman, Rev. Mod. Phys. **75**, 543 (2003).

[7] J. J. Larsen, K. Hald, N. Bjerre, H. Stapelfeldt, and T. Seideman, Phys. Rev. Lett. **85**, 2470 (2000).

[8] H. Tanji, S. Minemoto, and H. Sakai, Phys. Rev. A **72**, 063401 (2005).

[9] I. Nevo, L. Holmegaard, J. H. Nielsen, J. L. Hansen, H. Stapelfeldt, F. Filsinger, G. Meijer, and J. Kupper, Phys. Chem. Chem. Phys. **11**, 9912 (2009).

[10] J. G. Underwood, B. J. Sussman, and A. Stolow, Phys. Rev. Lett. **94**, 143002 (2005).

[11] K. F. Lee, D. M. Villeneuve, P. B. Corkum, A. Stolow, and J. G. Underwood, Phys. Rev. Lett. **97**, 173001 (2006).

[12] A. Rouzée, S. Guérin, O. Faucher, and B. Lavorel, Phys. Rev. A **77**, 043412 (2008).

[13] X. Ren, V. Makhija, and V. Kumarappan, Phys. Rev. Lett. **112**, 173602 (2014).

[14] S. S. Viftrup, V. Kumarappan, S. Trippel, H. Stapelfeldt, E. Hamilton, and T. Seideman, Phys. Rev. Lett. **99**, 143602 (2007).

[15] S. S. Viftrup, V. Kumarappan, L. Holmegaard, C. Z. Bisgaard, H. Stapelfeldt, M. Artamonov, E. Hamilton, and T. Seideman, Phys. Rev. A **79**, 023404 (2009).

[16] A. Korobenko and V. Milner, Phys. Rev. Lett. **116**, 183001 (2016).

[17] J. G. Underwood, M. Spanner, M. Y. Ivanov, J. Mottershead, B. J. Sussman, and A. Stolow, Phys. Rev. Lett. **90**, 223001 (2003).

[18] D. Takei, J. H. Mun, S. Minemoto, and H. Sakai, Phys. Rev. A **94**, 013401 (2016).

[19] D. Pentlehner, J. H. Nielsen, A. Slenczka, K. Mølmer, and H. Stapelfeldt, Phys. Rev. Lett. **110**, 093002 (2013).

[20] D. Pentlehner, J. H. Nielsen, L. Christiansen, A. Slenczka, and H. Stapelfeldt, Phys. Rev. A **87**, 063401 (2013).

[21] L. Christiansen, J. H. Nielsen, D. Pentlehner, J. G. Underwood, and H. Stapelfeldt, Phys. Rev. A **92**, 053415 (2015).

[22] B. Shepperson, A. A. Søndergaard, L. Christiansen, J. Kaczmarczyk, R. E. Zillich, M. Lemeshko, and H. Stapelfeldt, Phys. Rev. Lett. **118**, 203203 (2017).

[23] B. Shepperson, A. S. Chatterley, A. A. Søndergaard, L. Christiansen, M. Lemeshko, and H. Stapelfeldt, J. Chem. Phys. **147** 013946 (2017).

[24] J. Harms, M. Hartmann, J. P. Toennies, A. F. Vilesov, and B. Sartakov, J. Mol. Spectrosc. **185**, 204 (1997).

[25] M. Y. Choi, G. E. Douberly, T. M. Falconer, W. K. Lewis, C. M. Lindsay, J. M. Merritt, P. L. Stiles, and R. E. Miller, Int. Rev. Phys. Chem. **25**, 15 (2006).

[26] J. C. H. Spence and R. B. Doak, Phys. Rev. Lett. **92**, 198102 (2004).

[27] R. M. P. Tanyag *et al.*, Structural Dynamics **2**, 051102 (2015).

[28] Y. He, J. Zhang, and W. Kong, J. Chem. Phys. **145**, 034307 (2016).

[29] J. P. Toennies and A. F. Vilesov, Angew. Chem., Int. Ed. **43**, 2622 (2004).

[30] S. Trippel, T. G. Mullins, N. L. M. Müller, J. S. Kienitz, K. Długołęcki, and J. Küpper, Mol. Phys. **111**, 1738 (2013).

[31] T. Kierspel *et al.*, J. Phys. B **48**, 204002 (2015).

[32] A. T. Eppink and D. H. Parker, Rev. Sci. Instrum. **68**, 3477 (1997).

[33] J. J. Larsen, H. Sakai, C. P. Safvan, I. Wendt-Larsen, and H. Stapelfeldt, J. Chem. Phys. **111**, 7774 (1999).

[34] J. Gagnon, F. L. Kevin, D. M. Rayner, P. B. Corkum, and V. R. Bhardwaj, J. Phys. B **41**, 215104 (2008).

[35] H. Hasegawa, A. Hishikawa, and K. Yamanouchi, Chem. Phys. Lett. **349**, 57 (2001).

[36] C. S. Slater, S. Blake, M. Brouard, A. Lauer, C. Vallance, C. S. Bohun, L. Christensen, J. H. Nielsen, M. P. Johansson, and H. Stapelfeldt, Phys. Rev. A **91**, 053424 (2015).

[37] L. Christensen, L. Christiansen, B. Shepperson, and H. Stapelfeldt, Phys. Rev. A **94**, 023410 (2016).

[38] J. L. Hansen, J. H. Nielsen, C. B. Madsen, A. T. Lindhardt, M. P. Johansson, T. Skrydstrup, L. B. Madsen, and H. Stapelfeldt, J. Chem. Phys. **136**, 204310 (2012).

[39] C. S. Slater, S. Blake, M. Brouard, A. Lauer, C. Vallance, J. J. John, R. Turchetta, A. Nomerotski, L. Christensen, J. H. Nielsen, M. P. Johansson, and H. Stapelfeldt, Phys. Rev. A **89**, 011401 (2014).

[40] See the Supplemental Material at http://link.aps.org/supplemental/10.1103/PhysRevLett.119.073202 for the discussion of the extraction of nonaxial recoil width for Cl^+ ions.

[41] J. Ortigoso, M. Rodríguez, M. Gupta, and B. Friedrich, J. Chem. Phys. **110**, 3870 (1999).

[42] H. Sakai, C. P. Safvan, J. J. Larsen, K. M. Hilligsœ, K. Hald, and H. Stapelfeldt, J. Chem. Phys. **110**, 10235 (1999).

[43] R. Torres, R. de Nalda, and J. P. Marangos, Phys. Rev. A **72**, 023420 (2005).

[44] S. Trippel, T. Mullins, N. L. M. Müller, J. S. Kienitz, J. J. Omiste, H. Stapelfeldt, R. González-Férez, and J. Küpper, Phys. Rev. A **89**, 051401 (2014).

[45] D. M. Villeneuve, S. A. Aseyev, P. Dietrich, M. Spanner, M. Y. Ivanov, and P. B. Corkum, Phys. Rev. Lett. **85**, 542 (2000).

[46] S. Yang and A. M. Ellis, Chem. Soc. Rev. **42**, 472 (2013).

[47] A. I. G. Flórez, D.-S. Ahn, S. Gewinner, W. Schöllkopf, and G. v. Helden, Phys. Chem. Chem. Phys. **17**, 21902 (2015).

[48] K. Nauta and R. E. Miller, Science **283**, 1895 (1999).